NREL
NATIONAL RENEWABLE ENERGY LABORATORY

Slope Error Measurement Tool for Solar Parabolic Trough Collectors

Preprint

J. Kathleen Stynes
University of Colorado at Boulder

Benjamin Ihas
National Renewable Energy Laboratory

To be presented at the 2012 World Renewable Energy Forum
Denver, Colorado
May 13–17, 2012

Conference Paper
NREL/CP-5500-54636
April 2012

Contract No. DE-AC36-08GO28308

Available electronically at http://www.osti.gov/bridge

Available for a processing fee to U.S. Department of Energy
and its contractors, in paper, from:

U.S. Department of Energy
Office of Scientific and Technical Information
P.O. Box 62
Oak Ridge, TN 37831-0062
phone: 865.576.8401
fax: 865.576.5728
email: mailto:reports@adonis.osti.gov

Available for sale to the public, in paper, from:

U.S. Department of Commerce
National Technical Information Service
5285 Port Royal Road
Springfield, VA 22161
phone: 800.553.6847
fax: 703.605.6900
email: orders@ntis.fedworld.gov
online ordering: http://www.ntis.gov/help/ordermethods.aspx

Cover Photos: (left to right) PIX 16416, PIX 17423, PIX 16560, PIX 17613, PIX 17436, PIX 17721

Printed on paper containing at least 50% wastepaper, including 10% post consumer waste.

SLOPE ERROR MEASUREMENT TOOL FOR SOLAR PARABOLIC TROUGH COLLECTORS

J. Kathleen Stynes
PhD. Candidate Dpt. Mechanical Engineering
University of Colorado at Boulder
Boulder, Colorado 80301
Email: stynesj@colorado.edu

Benjamin Ihas
Thermal Systems Group
National Renewable Energy Laboratory
Golden, Colorado, 80401
Benjamin.Ihas@nrel.gov

ABSTRACT

The National Renewable Energy Laboratory (NREL) has developed an optical measurement tool for parabolic solar collectors that measures the combined errors due to absorber misalignment and reflector slope error. The combined absorber alignment and reflector slope errors are measured using a digital camera to photograph the reflected image of the absorber in the collector. Previous work using the image of the reflection of the absorber finds the reflector slope errors from the reflection of the absorber and an independent measurement of the absorber location. The accuracy of the reflector slope error measurement is thus dependent on the accuracy of the absorber location measurement. By measuring the combined reflector-absorber errors, the uncertainty in the absorber location measurement is eliminated. The related performance merit, the intercept factor, depends on the combined effects of the absorber alignment and reflector slope errors. Measuring the combined effect provides a simpler measurement and a more accurate input to the intercept factor estimate. The minimal equipment and setup required for this measurement technique make it ideal for field measurements.

1 INTRODUCTION

As we pursue efforts to lower the capital and installation costs of parabolic trough solar collectors, it is essential to maintain high optical performance. The geometric accuracy of parabolic trough collectors is described by the intercept factor, which includes the optical effects of reflector shape and receiver absorber alignment among others. The Distant Observer (DO) method, originally outlined by Wood in 1981, provides a means to measure optical performance of concentrating solar power plants in the field. The National Renewable Energy Laboratory (NREL) is currently developing a prototype DO system that measures the combined absorber alignment and reflector slope errors. The DO method uses digital photography of the reflection of the absorber as seen in the reflector to quantify the geometric alignment of the collector. This method is easily scalable to measure full solar fields at concentrating solar power plants.

2 PREVIOUS WORK

It was first recognized in 1981 by Wood that a great deal of information could be ascertained by analyzing the reflection of the absorber tube in parabolic trough collectors [1]. Just as parallel rays from the sun are reflected off a parabolic trough onto the absorber, so are the lines of sight from an observer reflected onto the absorber tube. Thus an observer aligned with the optical axis of the collector sees the reverse, an enlarged image of the absorber on the reflective surface. Wood's method utilizes the shape of this reflected image to ascertain detailed information about the optical performance of the collector.

The German Aerospace Center (DLR) has successfully implemented a quantitative variation of Wood's method to measure slope errors of parabolic troughs from the reflected absorber image [2] and [3]. The method uses high-resolution digital photography. A series of photographs is taken of the collector from either the ground (first publication) or a radio-controlled helicopter (second publication). In the original paper, the absorber location and camera position on the ground are measured with a laser distance meter. Most recently, the camera position in the air is determined using photogrammetric resection based on a series of ground control targets placed around the collector. The authors do not disclose their method for measuring the absorber position for the airborne technique. In all of these techniques, the uncertainty in the reflector slope errors depends on the uncertainty in the ab-

sorber location measurement. In each case, the absorber location is measured independently and then used along with images of the reflection of the absorber to find the reflector slope errors.

3 THEORY

A parabolic trough is a type of concentrating solar thermal technology. Concentrating solar power (CSP) uses a reflector to focus direct-normal solar radiation onto a receiver. The conventional solar trough tracks the sun during the day by rotating about a single axis. Typical collectors track the sun from east to west by rotating about a north-south axis. A reflective surface formed in the shape of a parabola focuses solar rays onto a cylindrical receiver located at the focal line. The receiver is comprised of an absorber tube surrounded by a glass envelope. A vacuum is drawn in the annulus between these two tubes in order to minimize heat losses to the environment. Figure. 1 shows a cross-section of a parabolic trough collector.

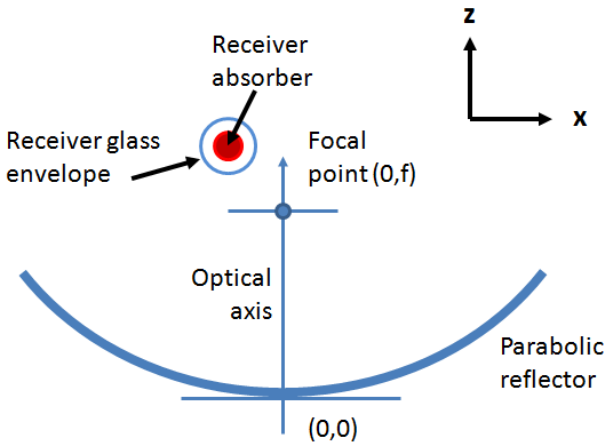

Fig. 1. Labeled schematic of a parabolic trough collector

3.1 Intercept Factor

The efficiency of a concentrating solar collector varies with the level of direct-normal solar radiation and the absorber temperature. However, due to the difficulty of measuring the absorber temperature directly, the efficiency is usually expressed as a function of the heat transfer fluid temperature with a single curve for each level of direct-normal solar radiation. As shown in Fig. 2, the optical losses far outweigh the thermal losses in the typical operating temperature range.

Because the thermal and optical efficiencies behave nearly independently, the optical performance of a solar concentrator can be treated separately from the thermal performance.

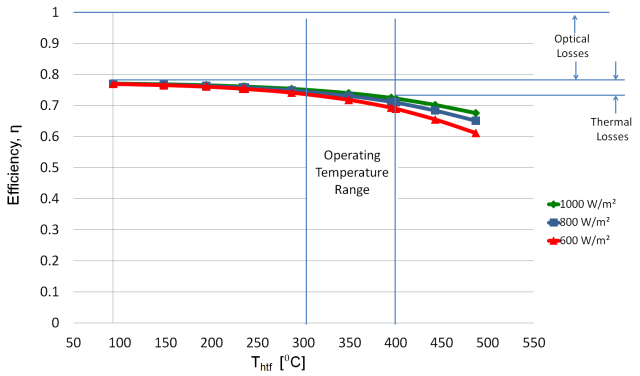

Fig. 2. Efficiency curve for parabolic trough solar collector comparing optical losses to thermal losses

The optical efficiency at normal incidence is the product of the intercept factor γ, the mirror reflectance ρ, the glass transmittance τ, and the absorber absorptance α.

$$\eta_o = \gamma\rho\tau\alpha \tag{1}$$

While the reflectance, transmittance, and absorptance are material properties that can be measured in a laboratory, the intercept factor is a purely geometric quantity that characterizes the total geometric accuracy of the system and is defined as the fraction of solar energy reflected from the concentrator that is intercepted by the absorber tube.

The intercept factor depends on several components including the reflector's surface profile or slope, reflector's specularity, reflector's alignment, absorber's alignment, and the system's solar tracking error. Additionally, factors that influence the intercept factor that are difficult to measure or dynamic in time include wind loading, gravitational loading, and sun shape. While the intercept factor is of utmost significance when evaluating the performance of a parabolic solar collector, it is difficult to measure due to its many contributing factors. Of all these factors, the greatest emphasis is usually placed on the reflector's profile, characterized by surface slope. Several optical tools exist to measure the slope errors of the reflecting surface including VSHOT [4], SOFAST [5], photogrammetry [6], and TARMES [2]. Upon measuring the reflector's slope, an estimate of the collector's intercept factor is often presented with the results. The other parameters included in the intercept factor are usually estimated at the researcher's discretion. There is no standard regarding the inclusion of specific parameters, let alone their default values.

In order to improve the accuracy of the intercept factor estimate, the Distant Observer method is capable of measuring the combined errors in the reflector's surface slope and the absorber's alignment. This not only provides additional measurement data for the intercept factor estimate, but also

reduces the overall measurement uncertainty since the independent measurement of the absorber location is eliminated.

3.2 Reflector Surface Slope Errors

For an ideal parabola, all incoming rays parallel to the optical axis (normal rays) will be reflected through the focal point of that parabola. A surface slope error is defined as the angular difference between the measured surface normal and the ideal surface normal of the design parabolic surface. The transverse slope errors are of much greater significance than the longitudinal slope errors because parabolic troughs are linear concentrators. The Distant Observer method only measures transverse slope errors. The transverse slope is defined perpendicular to the length of the collector and the longitudinal slope is defined parallel to the length of the collector. The Distant Observer measurement principle for measuring only slope errors is depicted in Fig. 3. For an absorber aligned with the focal line of the collector, the slope error at each point on the collector can be measured by finding the angle of an incoming ray that is reflected through the focal point of the collector. The slope error, θ_r, is equal to half of the angular difference between the incoming ray and a normal ray.

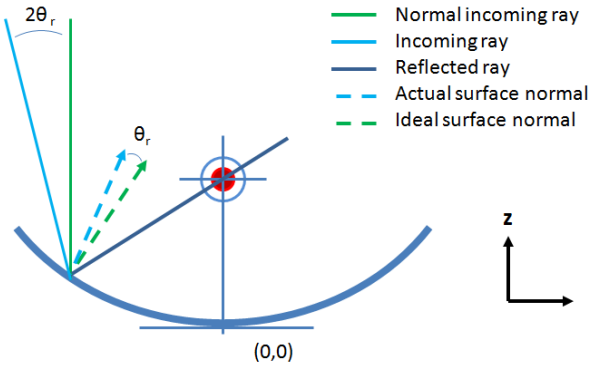

Fig. 3. Graphical representation of a reflector surface slope error using ray-tracing

3.3 Absorber Alignment Errors

An absorber misalignment must be modeled as a distribution of effective slope errors in order to combine the effects of absorber misalignment and reflector slope. For a perfect reflector with no surface slope errors, an incoming ray, assumed to be parallel to the optical axis, will be reflected and pass through the focal point of the parabola as shown in Fig. 4 (labeled as "ideal reflection"). For an incoming ray to pass through the center of an absorber that is not aligned with the focal point, the reflector surface must have nonzero slope error. An absorber misalignment can thus be modeled as a perfectly aligned absorber and a set of effective slope errors in the reflector surface. The effective slope error, θ_a, at each point across the aperture is determined by finding the surface slope error required for an incoming solar ray to intersect the center of the absorber instead of the focal point. The effective slope error is equal to half of the angle between the absorber tube, the point on the aperture, and the focal point as shown in Fig. 4. For a known absorber location, (X_a, Z_a), the effective slope error at a point on the parabolic trough reflector, (X_t, Z_t), of a parabolic collector with focal point $(0, f)$ is calculated using Eqn. 2.

$$\theta_a = \frac{1}{2}\left[\tan^{-1}\left(\frac{X_t - 0}{Z_t - f}\right) - \tan^{-1}\left(\frac{X_t - X_a}{Z_t - Z_a}\right)\right] \qquad (2)$$

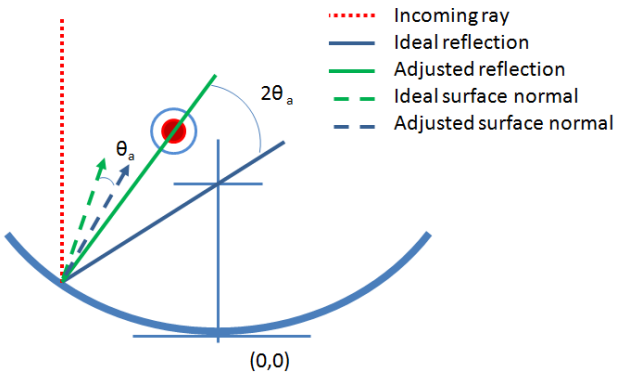

Fig. 4. Depiction of absorber misalignment represented with effective slope errors

3.4 Reflector-Absorber Errors

The reflector surface slope errors are combined with the effective slope errors due to absorber misalignment in the reflector-absorber errors. To combine the reflector surface slope errors with the absorber alignment errors, the absorber misalignment is modeled as a distribution of effective slope errors. The effective slope errors caused by absorber misalignment, θ_a, can then be directly added to the reflector slope errors, θ_r, to calculate the combined reflector-absorber errors, θ_{ra}. The reflector-absorber errors are treated in the same manner as surface slope errors when estimating the intercept factor of a parabolic trough collector using ray tracing or convolution.

To summarize, a reflector surface slope error is the rotation in the surface normal of a real parabola required for a normal ray to be reflected through the focal point. An effective slope error caused by absorber misalignment is the rotation in the surface normal of an ideal parabola required for a normal ray to be reflected through the center of the absorber. A reflector-absorber error is the rotation in the surface normal of a real

parabola required for a normal ray to be reflected through the center of the absorber.

3.5 Camera Model

In order to use a camera as a tool to measure the absorber alignment, the camera must be well characterized. Traditionally, cameras are modeled using a perspective-center model to which both radial and tangential lens distortions are applied. The perspective-center model is based on the principle of collinearity; that is, a point in object space, the corresponding point on the image sensor (image space), and the focal point of the camera all lay on a straight line. Object space is the 3D space containing the objects that you are photographing, while image space is the 2D image sensor in the camera. The principle of collinearity allows the location of points in object space to be determined from their corresponding locations in image space. Figure 5 illustrates the perspective-center camera model. The object point $(X_\mathrm{p}, Y_\mathrm{p}, Z_\mathrm{p})$ is imaged by the real camera on the sensor at point $(x'_\mathrm{p}, y'_\mathrm{p})$. This image point must be corrected by the lens distortion components $(\delta_\mathrm{x}, \delta_\mathrm{y})$ so that it is imaged by the perspective-center camera at point $(x_\mathrm{p}, y_\mathrm{p})$. The sensor size ($s_\mathrm{x}$ x s_y) is the length and height of the image sensor. The perspective center is the point through which all straight lines pass. The principal point (x_0, y_0) is the intersection of the image sensor and a line perpendicular to the image sensor passing through the perspective center. The focal length (f_c) is the normal distance between the image sensor and the perspective center.

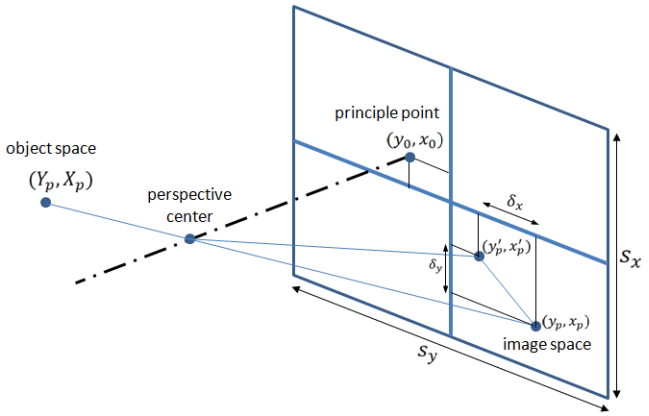

Fig. 5. Perspective-center model of a camera [7]

The lens distortion quantifies the deviation of rays from the ideal central-perspective model in a real camera and is expressed as deviations $(\delta_\mathrm{x}, \delta_\mathrm{y})$ in the image plane. The following lens distortion model is summarized from [8]. The primary types of lens distortion are radial distortion and tangential distortion. Radial distortion accounts for the majority of lens aberrations and has radial symmetry, while tangential distortion is mainly caused by decentering or misalignment of lens elements. Three radial distortion coefficients (K_1, K_2, and K_3) are usually sufficient to characterize the radial components of distortion.

$$\begin{aligned} \delta_{\mathrm{x_r}} &= x'(K_1 r^2 + K_2 r^4 + K_3 r^6) \\ \delta_{\mathrm{y_r}} &= y'(K_1 r^2 + K_2 r^4 + K_3 r^6) \end{aligned} \tag{3}$$

Any point (x', y') on the image sensor can be described as

$$r = \sqrt{x'^2 + y'^2} \tag{4}$$

Two tangential distortion coefficients (P_1 and P_2) are used to determine the tangential components of distortion.

$$\begin{aligned} \delta_{\mathrm{x_t}} &= P_1(r^2 + 2x'^2) + 2P_2 x' y' \\ \delta_{\mathrm{y_t}} &= P_2(r^2 + 2y'^2) + 2P_1 x' y' \end{aligned} \tag{5}$$

The radial and tangential components of lens distortion are summed to determine the total distortion displacement in each direction.

$$\begin{aligned} \delta_\mathrm{x} &= \delta_{\mathrm{x_r}} + \delta_{\mathrm{x_t}} \\ \delta_\mathrm{y} &= \delta_{\mathrm{y_r}} + \delta_{\mathrm{y_t}} \end{aligned} \tag{6}$$

To correct for lens distortion the pixel positions are shifted by the total distortion displacement values. This transforms the image to emulate one obtained by a central perspective camera.

$$\begin{aligned} x &= x' + \delta_\mathrm{x} \\ y &= y' + \delta_\mathrm{y} \end{aligned} \tag{7}$$

Therefore, a point in object space (X, Y, Z) will appear on the real camera's sensor in image space at (x', y'). Once the camera is modeled as a perspective-center camera, where the point in object space, the focal point, and the point in image space are collinear, the point in image space is corrected to be located at (x, y). A photograph that appears as though it were taken with a perspective-center camera is called an ideal photograph. Real photographs can be corrected to ideal photographs after a camera calibration is used to quantify the camera geometry.

4 METHOD

A reflector-absorber error is defined as the rotation in the surface normal of a real parabola at a point on the collector required for a normal ray (parallel to the optical axis) to be

reflected through the center of the absorber. The reflector-absorber errors can be calculated by determining the angle of an incoming ray that passes through the center of the absorber. The reflector-absorber error at any point on the collector is equal to half the angular difference between an incoming ray that is reflected through the center of the absorber and the optical axis of the collector. To calculate the reflector-absorber errors, a series of photographs of the collector showing the reflected image of the absorber are taken. Each photograph is analyzed to determine where on the aperture the center of the reflection of the absorber is located. The location of the camera relative to the collector is determined using photogrammetry and provides the angles of the incoming rays.

4.1 Taking the Photographs

The Distant Observer measurement consists of taking a series of photographs of a parabolic trough solar collector at different angles with respect to the optical axis of the collector. In general, each photograph should show the entire collector module. The photographs should begin with the reflection of the absorber not visible in the collector, as the angle of the camera with respect to the collector changes the reflection of the absorber should appear on one side of the aperture and move across the entire aperture until it is no longer visible. Ideally, the angles at which the photographs are taken should be evenly spaced. There are two options for obtaining the required images: move the camera across the aperture of a stationary collector or hold the camera stationary and rotate the collector.

4.2 Camera Calibration

In order to use the camera as a measurement device, the camera must be calibrated. A complete camera calibration quantifies the focal length, sensor size, principal point of the camera, and both the radial and tangential lens distortion coefficients (as described in Section 3.5). Specifications provided by the camera manufacturer for sensor size and focal length are approximations and should not be used in calculations; these values should always be determined with a camera calibration. Once the camera calibration has been performed, the images can be corrected for lens distortion.

The camera is calibrated by taking images of a calibration target. A grid of dots or a black and white checkerboard, as shown in Fig. 6, are convenient targets for calibration. A camera calibration toolbox for Matlab developed by CalTech is available online [9], or a commercial software package, such as PhotoModeler [10], can be purchased to perform the calibration. Other commercial photogrammetry software packages exist that are capable of performing camera calibrations, but the authors' experience is limited to the previously mentioned options. Specific guidelines for each of the aforementioned camera calibration platforms are provided with each software package. Once the camera has been calibrated, each photograph can be corrected for lens distortion as described in Section 3.5.

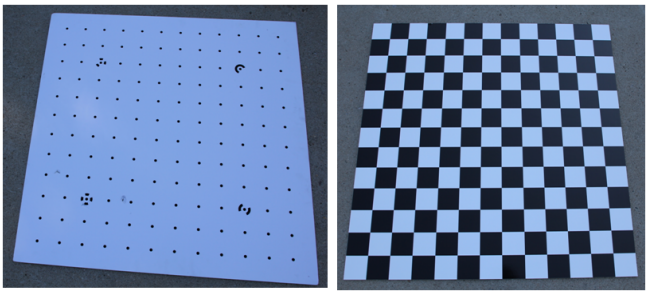

Fig. 6. Photographs of example calibration targets

4.3 Locating the Camera

The camera location is determined using photogrammetry. Photogrammetry uses the concept that a point in object space, the perspective center of the camera, and the corresponding point in image space all lie on the same line. Identifiable points in object space that are visible in multiple photographs are used as the targets. Targets are classified either as intentional targets which are designed for maximum accuracy and placed on and around the collectors specifically for this measurement or natural targets which are any naturally occurring distinguishable features on the collector. Intentional targets are typically black circular targets mounted on a white background. Manufacturer identifying stickers that can often be found on many of the mirror panels make good natural targets as do the corners of the mirror panels.

To find the camera location, the method of least squares bundle adjustment is used as described in *The Manual of Photogrammetry* 4th ed. [11]. The bundle adjustment technique uses photographs that have already been corrected for lens distortion through a camera calibration. The camera locations and target locations in object space are found simultaneously using the collinearity equations (Eqn. 8) in order to minimize the residuals in target locations in image space.

$$\begin{aligned} x - x_0 &= -f_c \frac{r_{11}(X - X_c) + r_{12}(Y - Y_c) + r_{13}(Z - Z_c)}{r_{31}(X - X_c) + r_{32}(Y - Y_c) + r_{33}(Z - Z_c)} \\ y - y_0 &= -f_c \frac{r_{21}(X - X_c) + r_{22}(Y - Y_c) + r_{23}(Z - Z_c)}{r_{31}(X - X_c) + r_{32}(Y - Y_c) + r_{33}(Z - Z_c)} \end{aligned} \tag{8}$$

When solving a system of equations it is important to keep track of the number of unknowns and the number of equations to make sure that the system is not under speci-

fied. Each photograph introduces six unknowns: the external orientation parameters, which are the camera location (X_c, Y_c, Z_c) and the Euler angle rotation of the camera $(\theta_\alpha, \theta_\beta, \theta_\gamma)$. Each object point introduces three unknowns: the three point coordinates (X_p, Y_p, Z_p). Two observation equations can be written for each point on each photograph. For M photographs and N points, there will be $6M + 3N$ unknowns and $2MN$ equations. If there are more unknowns than equations, the additional required equations must come from constraint equations. A constraint equation provides measured values for known locations of targets in object space, known distances, and other known geometric constraints.

Regardless of the number of photographs and object points, it is necessary to define the coordinate system with constraint equations. A minimum of seven constraint equations are required for this task. Three constraints define the origin or translation of the coordinate system, three constraints define the axes or rotation, and the seventh constraint defines the scaling. A minimum of three object points are used in the constraint equations to specify the coordinate system. For example, Fig. 7 shows a parabolic collector with three object points on the corners of the collector. With the object points labeled $j = 1, 2, 3$, we specify (X_1, Y_1, Z_1), (X_2, Z_2), (Z_3), and the distance between points 1 and 2. Typically, the design conditions give $Z_1 = Z_2 = Z_3$ and $X_1 = X_2$. The distance between points 1 and 2 is measured with a laser distance meter to provide the final scaling constraint. The accuracy of

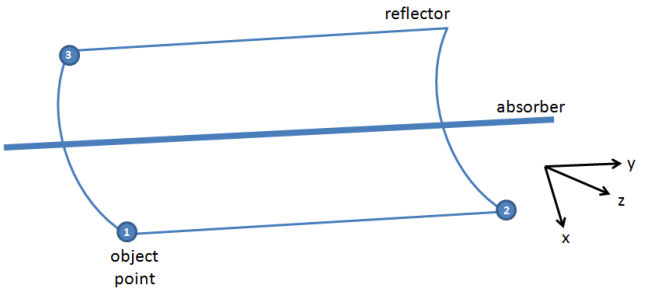

Fig. 7. Schematic of Parabolic Collector with three object points on the corners

the camera location depends primarily on the accuracy of the distance measurement, the number of targets visible in each photograph, and the accuracy to which each target can be located in the photographs.

4.4 Reflection of the Absorber

Once the camera locations are known, the surface of the reflector must be found in each photograph. The surface of the design parabola is discretized with a regular grid of points as shown in Fig. 8. The regular grid of points can be projected onto a photograph by solving the collinearity equations (Eqn. 8) explicitly for the corresponding image points on the sensor (x_p, y_p). Points in image space can be converted to pixel space (x_I, y_I) by shifting them by half the sensor length and then scaling by the ratio of the number of pixels (N_p) to the length of the sensor (s) (Eqn. 10).

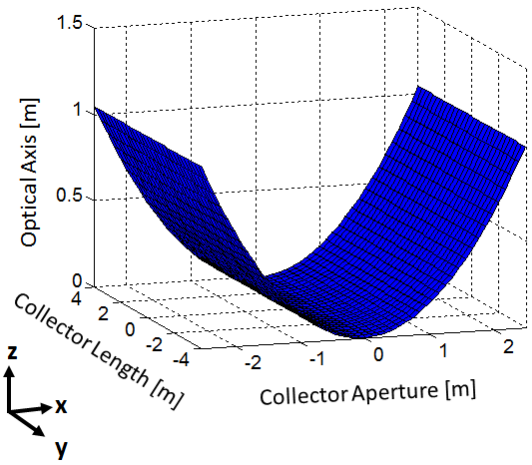

Fig. 8. Regular grid of points discretizing the design parabolic collector

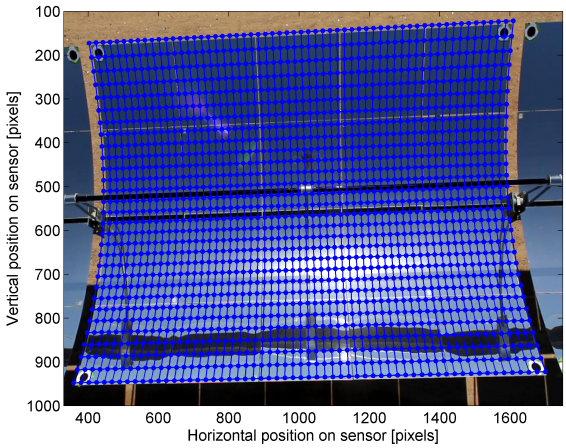

Fig. 9. Ideal photograph with regular grid of point projected onto the collector

$$x_I = \left(x_p + \frac{s_x}{2}\right) \frac{N_{px}}{s_x} \tag{9}$$

$$y_I = \left(y_p + \frac{s_y}{2}\right) \frac{N_{py}}{s_y} \tag{10}$$

Figure 9 shows a photograph of a collector with the reflector discretization superimposed. The intensity values at the location of each point on the reflector are determined by interpolating the intensity values in the photograph. Re-sampling the photograph along the grid of points corrects for the ef-

fects of parallax and results in an image of the reflector where the location of each image pixel is known in object space. Figure 10 shows the resulting image of the reflector. The reflection of the absorber can be seen clearly near the bottom of the collector. The location of the reflected image of the absorber on the aperture can be found directly from this parallax-corrected image.

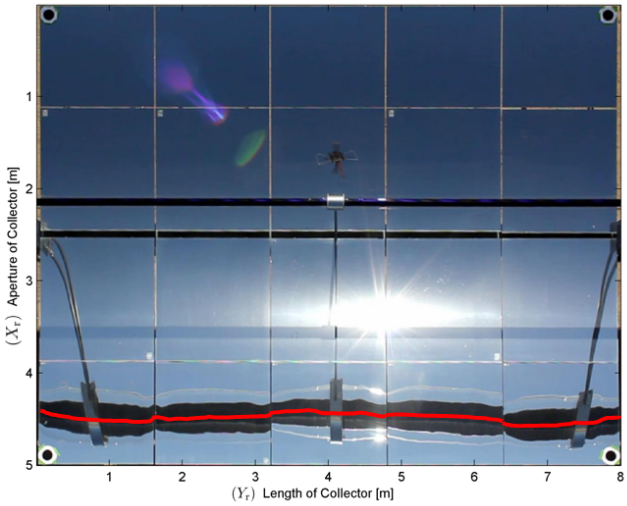

Fig. 10. Parallax corrected photograph of the reflector surface with centerline of the absorber superimposed in red

4.5 Reflector-Absorber Errors

The reflector-absorber errors are calculated from the location of the camera and the location of the reflection of the absorber. The intersection point on the reflector of an incoming ray that is reflected through the center of the absorber is found in the parallax-corrected image as the center of reflected image of the absorber (shown in red in Fig. 10). The reflector-absorber angle (θ_{ra}) is equal to the half of the angle between the incoming ray that is reflected through the center of the absorber and a normal ray (Eqn. 11).

$$\theta_{ra} = \frac{1}{2}\tan^{-1}\frac{X_c - X_r}{Z_c - Z_r} \tag{11}$$

where X_r is found on each parallax-corrected image as a function of length (Y_r) and Z_r is calculated from the design parabola. The camera location corresponding to that photograph (X_c, Z_c) was found previously using least squares bundle adjustment. By locating the center of the reflection of the absorber on each photograph, the reflector-absorber errors can be found across the entire collector.

5 UNCERTAINTY

The uncertainty in the measurement of the reflector-absorber errors depends on the interaction of many different variables. To evaluate the uncertainty for typical testing conditions, a detailed model was constructed in order to perform a Monte Carlo uncertainty analysis. The model uses ray tracing to create photographs of the reflector, absorber, and reflection of the absorber for known camera positions, collector geometry, and reflector-absorber errors. The photographs are analyzed with random errors in the collector geometry, camera calibration, target locations, and constraint parameters to determine the reflector-absorber errors. The calculated reflector-absorber errors are then compared to the initial input reflector-absorber errors to determine the measurement error. The whole photograph generation and analysis process is repeated to find the measurement uncertainty as a function of the random errors.

The camera selected is a CCD camera that takes high definition video at 1920x1080 pixels. The camera is moved virtually across a stationary collector with photographs generated every 5 cm. To locate the camera using least squares bundle adjustment, six target coordinates are provided as constraints as described in section 4.3. The collector design is typically used to determine values for these target constraints; however, if the collector does not conform perfectly to design there will be errors in the target constraints. The target constraint errors are estimated to be $\sigma = \pm 5$ mm. The difference between the focal length of the collector used to generate the images and the focal length of the collector used to analyze the images is $\sigma = \pm 5$ mm. Using intentional targets, the target centroid location can be found to within $\sigma = \pm 0.1$ pixels and when using natural targets, the target centroid error is limited to $\sigma = \pm 1$ pixels.

The input reflector-absorber errors used to generate the photographs consist of an absorber that is misaligned from the focal line by 3 mm towards the rim of the collector ($X_a = 3$ mm) and 5 mm towards the vertex of the collector ($Z_a = -5$ mm). The sinusoidal pattern given in Eqn. 12 was used as the input reflector slope errors.

$$\theta_r = 0.003\left[\sin\left(4Y_t\right)\sin\left(4X_t\right)\right] \tag{12}$$

Figure 11 shows the cumulative probability plot of the errors in the calculation of the reflector-absorber errors. That is, the plot shows the absolute value of the difference between the input reflector-absorber errors used to generate images and the reflector-absorber errors calculated during the image analysis. Each line in the cumulative probability plot represents the average of 30 model runs for a different value of error in the target image points. Figure 11 shows the differ-

ence in measurement accuracy when using intentional targets ($\sigma = 0.1$ pixels) and natural targets ($\sigma = 1$ pixel). The uncertainty in the reflector-absorber errors for intentional targets is ± 0.78 mrad and ± 0.90 mrad for natural targets with 95% confidence. While using intentional targets provides a slightly more accurate measurement, both intentional and natural targets can be used to measure the reflector-absorber errors to within ± 1 mrad (95% confidence).

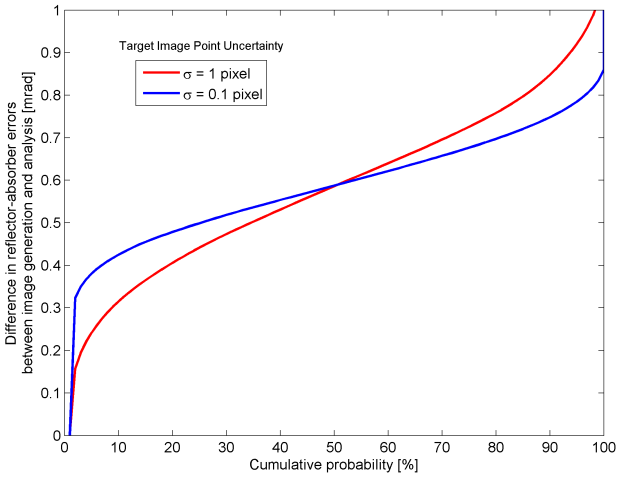

Fig. 11. Cumulative probability of the uncertainty in the calculated reflector-absorber errors (averaged over 30 model runs) using typical random errors described above and noted target image point location errors

6 Conclusions

The Distant Observer Method has been adapted to measure the combined errors due to reflector slope errors and absorber misalignment errors. The combined errors are termed the reflector-absorber errors and are defined as the rotation of the surface normal in the transverse direction required for an incoming ray parallel to the optical axis to be reflected through the center of the absorber. The reflector-absorber errors are measured by taking a series of photographs of the reflected absorber image at incremental locations across the aperture of the collector. The images are analyzed to find the camera location using photogrammetric bundle adjustment. The calculated camera location is used along with the location of the reflection of the absorber to determine the reflector-absorber errors. The uncertainty in the reflector-absorber errors for typical measurement conditions was found using a detained model. Under typical measurement conditions the reflector-absorber errors can be found to within ± 0.78 for intentional targets that are placed on the collector and ± 0.90 for natural targets such as the mirror edge corners. The Distant Observer measurement technique can be applied in the field to improve the estimate of optical intercept factor.

ACKNOWLEDGMENT

This work was supported by the U.S. Department of Energy under Contract No. DE-AC36-08-GO28308 with the National Renewable Energy Laboratory.

REFERENCES

[1] Wood, R., 1981. Distant observer techniques for verification of solar concentrator optical geometry. Tech. Rep. UCRL-53220, Lawrence Livermore National Laboratory, Oct.

[2] Ulmer, S., Heinz, B., Pottler, K., and Lüpfert, E., 2009. "Slope error measurements of parabolic troughs using the reflected image of the absorber tube". *Journal of Solar Energy Engineering,* **131**.

[3] Prahl, C., Stanicki, B., Hilgert, C., Ulmer, S., and Röger, M., 2011. "Airborne shape measurement of parabolic trough collector fields". In Proceedings of the 17th SolarPACES International Symposium.

[4] Wendelin, T., May, K., and Gee, R., 2006. "Video scanning hartmann optical testing of State-of-the-Art parabolic trough concentrators". In Proceedings of the ASME 2006 International Solar Energy Conferencer.

[5] Andraka, C. E., Sadlon, S., Myer, B., Trapeznikov, K., and Liebner, C., 2009. "Rapid reflective facet characterization using fringe reflection techniques". In Proceedings of the ASME 2009.

[6] Pottler, K., Lüpfert, E., Johnston, G. H., and Shortis, M. R., 2005. "Photogrammetry: A powerful tool for geometric analysis of solar concentrators and their components". *Journal of Solar Energy Engineering,* **127**, p. 94.

[7] Luhmann, T., Robson, S., Stephan, K., and Harley, I., 2006. *Close Range Photogrammetry*. Whittles Publishing, Scotland, UK.

[8] Brown, Duane, C., 1965. Advanced methods for the calibration of metric cameras. Tech. Rep. AD706870, DBA Systems Inc., Lanham, Maryland, Dec.

[9] Bouguet, J., 2010. Camera calibration toolbox for matlab. http://www.vision.caltech.edu/bouguetj/calib_doc/, July.

[10] Inc., E. S., 2011. PhotoModeler. http://www.photomodeler.com/index.htm.

[11] Wong, K. W., 1980. "Basic mathematics of photogrammetry". In *Manual of Photogrammetry*, C. Slama, C. Theurer, and S. Henriksen, eds., 4th ed. American Society of Photogrammetry and Remote Sensing.